An engineered 4-1BBL fusion protein with "activity on demand"

Mock, Jacqueline ; Stringhini, Marco ; Villa, Alessandra ; Weller, Michael ; Weiss, Tobias ; Neri, Dario

Abstract: Engineered cytokines are gaining importance in cancer therapy, but these products are often limited by toxicity, especially at early time points after intravenous administration. 4-1BB is a member of the tumor necrosis factor receptor superfamily, which has been considered as a target for therapeutic strategies with agonistic antibodies or using its cognate cytokine ligand, 4-1BBL. Here we describe the engineering of an antibody fusion protein, termed F8-4-1BBL, that does not exhibit cytokine activity in solution but regains biological activity on antigen binding. F8-4-1BBL bound specifically to its cognate antigen, the alternatively spliced EDA domain of fibronectin, and selectively localized to tumors in vivo, as evidenced by quantitative biodistribution experiments. The product promoted a potent antitumor activity in various mouse models of cancer without apparent toxicity at the doses used. F8-4-1BBL represents a prototype for antibody-cytokine fusion proteins, which conditionally display "activity on demand" properties at the site of disease on antigen binding and reduce toxicity to normal tissues.

DOI: https://doi.org/10.1073/pnas.2013615117

Main Manuscript for

An engineered 4-1BBL fusion protein with “activity-on-demand”

Jacqueline Mock[a], Marco Stringhini[a], Alessandra Villa[b], Michael Weller[c], Tobias Weiss[c], Dario Neri[a]*

[a]Department of Chemistry and Applied Biosciences, Swiss Federal Institute of Technology (ETH Zürich), Vladimir-Prelog-Weg 4, CH-8093 Zürich (Switzerland)

[b]Philochem AG, Libernstrasse 3, CH-8112 Otelfingen (Switzerland)

[c]Department of Neurology, University Hospital Zurich and University of Zurich, Frauenklinikstrasse 26, CH-8091 Zürich (Switzerland)

* corresponding author: Dario Neri

Email: neri@pharma.ethz.ch

ORCIDs

0000-0002-4618-1113

0000-0001-6807-0011

0000-0003-4070-286X

0000-0002-1748-174X

0000-0002-5533-9429

0000-0001-5234-7370

Classification

BIOLOGICAL SCIENCES/Applied Biological Sciences

Keywords

armed antibody, protein engineering, tumor targeting, 4-1BB, cancer immunotherapy

Author Contributions

D.N. and J.M. designed and planned the study. J.M. performed most of the experiments. M.S. helped with the biodistribution studies with radiolabeled proteins, designed the infiltrate analysis and helped to perform the experiment. A.V. coordinated immunohistochemical studies. T.W. and M.W. coordinated and performed the studies in glioblastoma. J.M. prepared the figures. D.N. and J.M. wrote the manuscript.

This PDF file includes:

Main Text

Abstract

Engineered cytokines are gaining importance for cancer therapy but those products are often limited by toxicity, especially at early time points after intravenous administration. 4-1BB is a member of the tumor necrosis factor receptor superfamily, which has been considered as a target for therapeutic strategies with agonistic antibodies or using its cognate cytokine ligand, 4-1BBL. Here we describe the engineering of an antibody fusion protein (termed F8-4-1BBL), which does not exhibit cytokine activity in solution but regains biological activity upon antigen binding. F8-4-1BBL bound specifically to its cognate antigen, the alternatively-spliced EDA domain of fibronectin, and selectively localized to tumors *in vivo*, as evidenced by quantitative biodistribution experiments. The product promoted a potent anti-tumor activity in various mouse models of cancer, without apparent toxicity at the doses used. F8-4-1BBL represents a prototype for antibody-cytokine fusion proteins, which conditionally display “activity-on-demand” properties at the site of disease upon antigen binding and reduce toxicity to normal tissues.

Significance Statement

Antibody-cytokine fusion proteins have been successfully applied for the treatment of preclinical models of cancer and yielded promising results in early clinical trials. The antibody moiety redirects the immunostimulatory payload to the tumor in order to boost the anti-tumor immune response. However, especially at early timepoints after administration, the relatively high concentration of the antibody-cytokine conjugate in blood can lead to severe side effects due to peripheral activation of cytokine receptors. Therefore, protein engineering approaches are necessary in order to develop antibody-cytokine conjugates that selectively regain their immunostimulatory activity upon antigen binding in the tumor. In this work, we have developed an antibody-cytokine conjugate that meets these criteria and which showed antitumor activity in preclinical models of cancer.

Main Text

Introduction

Cytokines are immunomodulatory proteins, which have been considered for pharmaceutical applications for the treatment of cancer patients(1-3) and other types of disease(2). There is a growing interest in the use of engineered cytokine products as anti-cancer drugs, capable of boosting the action of T cells and natural killer (NK) cells against tumors(3, 4), alone or in combination with immune check-point inhibitors(3, 5-7).

Recombinant cytokine products on the market include IL2 (Proleukin®)(8, 9), IL11 (Neumega®)(10, 11), TNF (Beromun®)(12), IFNα (Roferon A®, Intron A®)(13, 14), IFNβ (Avonex®, Rebif®, Betaseron®)(15, 16), IFNγ (Actimmune®)(17), G-CSF (Neupogen®)(18), GM-CSF (Leukine®)(19, 20). The recommended dose is typically very low (often at less than one milligram per day)(21-23), as cytokines may exert biological activity in the subnanomolar concentration range(24). In order to develop cytokine products with improved therapeutic index, various strategies have been proposed. Protein PEGylation or Fc fusions may lead to prolonged circulation time in the bloodstream, allowing the administration of low doses of active payload(25, 26). In some implementation, cleavable PEG polymers may be considered, yielding prodrugs which regain activity at later time points(27). Alternatively, tumor-homing antibody fusions have been developed, since the preferential concentration of cytokine payloads at the tumor site has been shown in preclinical models to potentiate therapeutic activity, helping spare normal tissues(28-34). Various antibody-cytokine fusions are currently being investigated in clinical trials for the treatment of cancer and of chronic inflammatory conditions [for reviews, see(2, 33, 35-37)].

Antibody-cytokine fusions display biological activity immediately after injection to patients, which may lead to unwanted toxicity and prevent escalation to therapeutically active dose regimens(9, 22, 38). In the case of pro-inflammatory payloads (e.g., interleukin-2, interleukin-12, tumor necrosis alpha), common side effects include hypotension, nausea and vomiting, as well as flu-like symptoms(24, 39-42). These side-effects typically disappear when the cytokine concentration drops below a critical threshold, thus providing a rationale for slow-infusion administration procedures(43). It would be highly desirable to generate antibody-cytokine fusion proteins with excellent tumor targeting properties and with “activity-on-demand” (i.e., with a biological activity which is conditionally gained upon antigen binding at the site of disease, helping spare normal tissues).

Here, we describe a novel fusion protein, consisting of the F8 antibody (specific to the alternatively-spliced EDA domain of fibronectin(44, 45)) and of murine 4-1BBL, which did not exhibit cytokine activity in solution but could regain potent biological activity upon antigen binding. The antigen is conserved from mouse to man(46), is virtually undetectable in normal adult tissues (exception made for placenta, endometrium and some vessels in the ovaries), but is expressed in the majority of human malignancies(44, 45, 47, 48). 4-1BBL is a member of the tumor necrosis factor superfamily(49). It is expressed on antigen-presenting cells(50, 51) and binds to its receptor 4-1BB which is upregulated on activated cytotoxic T cells(52), activated dendritic cells(52), activated NK and NKT cells(53) and on regulatory T cells(54). Signaling through 4-1BB on cytotoxic T cells protects them from activation-induced cell death and skews the cell towards a more memory-like phenotype(55, 56).

We engineered nine formats of the F8-4-1BBL fusion protein and one of them exhibited a superior performance in quantitative biodistribution studies and conditional gain of cytokine activity upon antigen binding. The antigen-dependent reconstitution of the biological activity of the immunostimulatory payload represents an example for an antibody fusion protein with “activity on demand”. The fusion protein was potently active against different types of cancer, without apparent toxicity at the doses used. ~~F8-4-1BBL may represent a prototype for next-generation antibody-cytokine fusions with “activity-on-demand”.~~ The EDA domain of fibronectin is a particularly attractive antigen for cancer therapy, in view of its high selectivity, stability and abundant expression in most tumor types(44, 45, 47, 48).

Results

Human 4-1BBL is a homotrimeric protein [**Figure 1a**](57), while its murine counterpart forms stable homodimers(58, 59). Stable trimeric structures can be engineered by connecting 4-1BBL monomeric domains with suitable polypeptide linkers(60). Recombinant antibodies can be expressed as full IgG or as fragments, forming single-chain Fv (scFv)(61, 62) or diabody(63) structures [**Figure 1b** and **Supplementary Table S1**](2, 64, 65). Nine different fusion proteins containing F8 antibody and murine 4-1BBL moieties were expressed in mammalian cells, in order to identify products with promising features for subsequent *in vivo* investigations. Mutational scans had revealed that the disulfide bond linking two 4-1BBL monomers is crucial for protein stability [**Supplementary Figure S1**]. The observation that the TNF homology domain (THD) within 4-1BBL was sufficient for full *in vitro* activity [**Supplementary Figure S2**] guided the design of the modules to be included in the fusion proteins. Six out of nine products exhibited favorable size exclusion and SDS-PAGE profiles [**Figure 1c** and **Supplementary Figure S3**]. We selected formats **2**, **3**, **5**, **7** and **8** for further investigations, since those proteins gave the best yields and did not show signs of aggregation even after repeated freeze-thaw cycles.

Figure 2 presents a comparative analysis of *in vitro* properties of F8-4-1BBL in various formats. The 4-1BBL and F8 moieties were able to recognize the cognate targets in the **2**, **3**, **5**, **7** and **8** formats. Indeed, all proteins bound with high affinity to murine CTLL-2 cells, which are strongly positive for murine 4-1BB (i.e., the 4-1BBL receptor) [**Figure 2a**] and to recombinant EDA domain of fibronectin [**Figure 2b**]. A functional assay with an NF-κB reporter cell line(66) revealed that all fusion proteins preferentially activated downstream signaling events in the presence of the cognate EDA fibronectin antigen, immobilized on a solid support and thus mimicking the tumor environment [**Figure 2c**]. Formats **5** [consisting of two disulfide-linked 4-1BBL monomeric units fused to scFv(F8)] and **8** [in which monomeric units of 4-1BBL were fused at the C-terminal ends of the heavy chains of IgG(F8)] exhibited the best discrimination between low biological activity in solution and high cytokine activity in the presence of antigen. For this reason, formats **5** and **8** were selected for an *in vivo* characterization of their tumor targeting properties. Format **2** was also included in the comparison, since diabody-based antibody cytokine fusion proteins have previously been used for clinical development programs(2, 64).

Protein preparations were radioiodinated and injected into immunocompetent 129/Sv mice, bearing subcutaneously-grafted murine F9 teratocarcinomas, which express EDA fibronectin around tumor blood vessels(44). Mice were sacrificed 24 hours after intravenous administration and biodistribution results were expressed as percent of injected dose per gram of tissue [%ID/g] [**Figure 3a and Supplementary Figure S4**]. Format **2** exhibited only a modest tumor uptake

(1.0% ID/g) and poor selectivity. Format **8** showed, as expected, a longer circulatory half-life, as evidenced by the high %ID/g in blood after 24 h, but the tumor uptake and selectivity were not significantly higher compared to KSF-4-1BBL (a fusion protein based on the KSF antibody, specific to hen egg lysozyme and serving as negative control(67)). By contrast, format **5** exhibited a preferential accumulation in the tumor (2.8 % ID/g) and a good tumor-to-normal organ selectivity. EDA targeting was essential for tumor homing, as revealed by the comparison of the biodistribution results with the negative control KSF-4-1BBL fusion protein [**Figure 3a and Supplementary Figure S4**]. In order to confirm selective tumor uptake with a different methodology, format **5** was injected into tumor-bearing mice. An *ex vivo* immunofluorescence analysis revealed a preferential accumulation of format **5** around tumor blood vessels, while no staining was detectable in normal organs or when the KSF fusion protein was used [**Figure 3b and Supplementary Figure S5**]. In line with previous reports on this matter(44, 45, 47, 48), the EDA-domain of fibronectin is an ideal target for pharmacodelivery applications in mouse and in man, as the antigen is undetectable in normal adult tissues, but is strongly expressed in the stroma and around the blood vessels in many different tumor types [**Supplementary Figure S6**].

Therapy studies were performed using format **5** of F8-4-1-BBL, both in a preventive setting starting at a tumor volume of 40 mm^3 and in a therapeutic setting starting at a tumor volume of 80 – 100 mm^3. In a preventive setting in WEHI-164 fibrosarcoma, three out of five mice rejected the tumor using F8-4-1-BBL as single agent, while four out of five mice showed a complete response when treated with PD-1 blockade, alone or in combination with F8-4-1-BBL [**Figure 4a**]. The cured mice rejected subsequent challenges with WEHI-164 fibrosarcoma cells. In some cured mice, a challenge with CT26 colon carcinoma cells was also rejected, similar to what we had previously reported for other F8-based immunocytokine therapeutics (68, 69)[**Supplementary Figure S7**]. When the therapy was repeated in mice bearing larger WEHI-164 fibrosarcoma tumors, a significant [$p = 0.0427$, regular two-way ANOVA, Tukey's multiple comparison test, day 13] tumor growth retardation was observed in mice treated with F8-4-1BBL [**Figure 4b**]. There was no difference in tumor growth between mice receiving injections of saline and the KSF fusion proteins, underlining the importance of the antigen-dependent activation of 4-1BBL [**Figure 4b**]. Similar experiments performed in immunocompetent mice bearing CT26 tumors showed a tumor regression in 4/5 mice treated with F8-4-1BBL. One mouse was cured, while tumors eventually regrew in the other mice. Therapy was potent also when F8-4-1BBL was combined with PD-1 blockade [**Figure 4c**]. All treatments in all experiments were well tolerated, as indicated by the absence of body weight loss [**Figure 4**]. When MC38 colon carcinoma-bearing mice were treated with F8-4-1BBL or PD-1 blockade as single agents, a moderate tumor growth retardation compared to mice treated with saline was observed [$p < 0.0001$, regular two-way ANOVA,

Tukey's multiple comparison test, day 13]. By contrast, the combination treatment was potently active and led to durable complete remissions in 2/6 mice [**Figure 4 d**].

To further investigate the therapeutic activity of F8-4-1BBL, alone or in combination with PD-1 blockade, we studied an orthotopic model of glioblastoma in immunocompetent mice. Treatment was started 5 days after intracerebral implantation of GL-261 tumor cells. Mice were imaged at day 12 by magnetic resonance imaging (MRI) and were monitored in terms of body weight and behavior. Mice were sacrificed when they developed neurologic symptoms. In keeping with previous reports, none of the mice from the saline treatment group survived more than 20 days. By contrast, F8-4-1BBL exhibited a potent anticancer activity, which was potentiated by PD-1 blockade. Eighty percent of the mice in the combination treatment group were rendered tumor-free, as evidenced both by MRI analysis and by survival data [**Figure 4e**].

In order to analyze the tumor infiltrating leukocytes, mice were sacrificed 48 h after the second cycle of injections. Tumors and tumor-draining lymph nodes were excised, homogenized and stained for analysis by flow cytometry. CT26 tumors were found to be highly infiltrated by lymphocytes, in keeping with previous reports(70-72), while WEHI-164 lesions were rather immunologically "cold" [**Figure 5a**]. The proportion of CD8+ T cells, specific to AH1 (a retroviral antigen, which plays a dominant role for the rejection of tumors implanted in BALB/c mice (69, 73)) was higher in CT26 tumors [**Figure 5a**]. Treatment with F8-4-1BBL led to a significant increase in intratumoral CD3+ T cell density in both models, but the proportion of CD4+ or CD8+ T cells did not vary substantially. No difference was observed in terms of regulatory T cell (T_{reg}) density [**Figure 5a**]. In keeping with what previously reported for other studies(74), the proportion of AH1-specific CD8+ T cells did not vary substantially as a result of pharmacological treatment [**Figure 5a**]. Treatment with F8-4-1BBL led to a decrease in CD3+ and CD4+ T cells in the tumor-draining lymph nodes with a concomitant increase of antigen-presenting cells in CT26 tumor-bearing mice (but not in WEHI-164) [**Figure 5b**]. An increase in the proportion of effector T cells (CD44+CD62L-) was observed among the AH1-specific CD8+ T cells in the tumor-draining lymph nodes [**Figure 5c**]. Virtually all tumor-infiltrating CD8+ T cells were positive for the exhaustion markers PD-1 and CD39 [**Figure 5c**](75, 76). The gating strategy used in the study can be found in **Supplementary Figure 7**. Collectively, the markers used in this study did not detect a phenotypic change in tumor-infiltrating T cells, but an increase in effector T cells was observed for the AH1-specific CD8+ T cell population in tumor-draining lymph nodes as a result of F8-4-1BBL treatment.

Discussion

We have described the development of an antibody-cytokine fusion protein targeted to the tumor neovasculature, featuring an engineered murine homodimeric 4-1BBL moiety as immunostimulatory payload. Some formats were completely inactive in solution while others retained a low biological activity in the absence of antigen. The low constitutive biological activity of the formats featuring two single-chain trimeric ligands could be due to a residual receptor clustering triggered by hexameric 4-1BBL. The size exclusion profile of Format **7** revealed the presence of a minor fraction of aggregated protein, which could potentially trigger some downstream signaling. However, since it was not possible to remove the aggregated fraction, this hypothesis could not be experimentally proven. Subtle variations in the molecular format were observed to not only lead to different performance *in vitro* but also affected the biodistribution properties *in vivo.* Both preferential localization in the tumor and antigen-dependent gain in activity are prerequisites for restricting the activity of the fusion protein to the site of disease. The selected format **5** was inactive in solution but regained activity upon clustering on the antigen. Favorable tumor-targeting results and potent tumor growth inhibition were observed *in vivo*, making F8-4-1BBL a promising prototype of for the development of next-generation immunocytokines with antigen-dependent activation properties.

4-1BB, the receptor for 4-1BBL has been recognized as important target for the immunotherapy of cancer, as this member of the TNF receptor superfamily delivers costimulatory signals to activated cytotoxic T cells(77). The first 4-1BB agonistic antibody, urelumab, showed promising anti-cancer activity in preclinical models, but unfortunately revealed substantial hepatotoxicity in clinical trials(78). The hepatic toxicity was mainly due to the activation of liver Kupffer cells and monocytes, leading to a massive infiltration by T cells(78, 79). Efforts are being made to develop 4-1BB agonists with more favorable toxicity profiles that retain potent costimulatory capacities(80-82). In addition to the optimization of anti-4-1BB immunoglobulins(80, 81), various formats of targeted 4-1BB agonists are being investigated. Bispecific antibodies capable of simultaneous recognition of 4-1BB and of tumor-associated antigens (e.g., EGFR or CEA) have been developed and tested in preclinical models of cancer, with encouraging results (82, 83). Novel formats of targeted 4-1BB agonists have recently been considered for clinical development. A FAP-targeted immunocytokine with trimeric single-chain 4-1BBL has recently started phase I clinical testing in cancer patients (84). A fusion protein of trastuzumab with a 4-1BB-specific anticalin™ has been described(85), which had shown antigen-dependent modulation of 4-1BB agonistic activity *in vitro* and which has recently started clinical trials(85).

The search for antibody-cytokine products with “activity-on-demand” has been recognized as an important research goal, in order to generate products with improved activity and safety profiles(86, 87). One possible strategy features the use of cytokine-binding polypeptides, acting as proteolytically-cleavable inhibitory moieties(88). Fusing cytokines at the C-terminal end of the IgG light chain may restrict conformational changes in the hinge region and slightly modulate cytokine activity upon antibody binding to the cognate antigen(87). The attenuation of cytokine potency by targeted mutagenesis has been considered as a strategy to increase the dose of antibody-cytokine fusion proteins(89) or to conditionally activate tumor cells which express both a tumor-associated antigen and a cytokine receptor (e.g., IFNα receptor) on their surface(90, 91). In addition, the targeted reconstitution of antibodies fused with “split-cytokine” moieties (i.e., subunits of heterodimeric cytokines that can reassemble at the tumor site) has been reported. Until now, the performance of that approach has been limited by the fact that the cytokine subunits used in the study (e.g., the p35 chain of IL12) retained biological activity(92).

Most ligands of the TNF superfamily including human 4-1BBL form homotrimers instead of homodimers as is the case for murine 4-1BBL(93). However, the activation of receptor of the TNF superfamily requires higher-order multimerization. The approach described in this article may be generally applicable to members of the TNF superfamily (60), if we were able to generate stable homodimers as payloads for antibody fusion. Alternative approaches may involve bispecific antibodies(94, 95), the modular use of small protein domains(85, 96) or of chemically-modified bicyclic peptides(97). Members of the TNF receptor superfamily are particularly suited for cooperative activation strategies in view of their homotrimeric structure and clustering-driven activation properties(98-100). The development of immunotherapeutics with “activity-on-demand” for monomeric cytokines may be more challenging, as one cannot rely on protein assembly for the reconstitution of biological activity.

Materials and Methods

Cell lines

The murine cytotoxic T cell line CTLL-2 (ATCC® TIB-214), the murine F9 teratocarcinoma cell line (ATCC® CRL-1720), the murine WEHI-164 fibrosarcoma cell line (ATCC® CRL-1751) and the murine CT26 colon carcinoma cell line (ATCC® CRL-2638) were obtained from ATCC. The MC38 colon carcinoma cell line was a kind gift from Prof. Onur Boyman (Department of Immunology, University Hospital Zurich, Zurich, Switzerland). The cells were expanded and stored as cryopreserved aliquots in liquid nitrogen. The CTLL-2 cells were grown in RPMI 1640 (Gibco, #21875034) supplemented with 10% FBS (Gibco, #10270106), 1 X antibiotic-antimycoticum (Gibco, #15240062), 2 mM ultraglutamine (Lonza, #BE17-605E/U1), 25 mM HEPES (Gibco, #15630080), 50 μM β-mercaptoethanol (Sigma Aldrich) and 60 U/mL human IL-2 (Proleukin, Roche Diagnostics). The F9 teratocarcinoma cells were grown in DMEM (Gibco, high glucose, pyruvate, #41966-029) supplemented with 10% FBS (Gibco, #10270106) and 1 X antibiotic-antimycoticum (Gibco, #15240062) in flasks coated with 0.1% gelatin (Type B from Bovine Skin, Sigma Aldrich, #G1393). The WEHI-164 fibrosarcoma and the CT26 colon carcinoma were grown in RPMI 1640 (Gibco, #21875034) supplemented with 10% FBS (Gibco, #10270106) and 1 X antibiotic-antimycoticum (Gibco, #15240062). The MC38 colon carcinoma cells were grown in Advanced DMEM (Gibco, #12491915) supplemented with 10% FBS (Gibco, #10270106), 1 X antibiotic-antimycoticum (Gibco, #15240062) and 2 mM ultraglutamine (Lonza, #BE17-605E/U1). GL-261 cells were obtained from the National Cancer Institute (Frederick, Maryland, USA) and cultured as previously described(101, 102). The cells were passaged at the recommended ratios and never kept in culture for more than one month.

Mice

Eight weeks old female C57BL/6, Balb/c and 129/Sv mice were obtained from Janvier. After at least one week of acclimatization, 10^7 F9 cells, 2.5 x 10^6 WEHI-164 cells, 4 x 10^6 CT26 or 10^6 MC38 cells were subcutaneously implanted into the right flank. The tumor size was monitored daily by caliper measurements and the volume was calculated using the formula [length x width x width x 0.5]. For mouse studies mouse models of glioblastoma, eight weeks old female C57BL/6 mice were purchased from Charles River Laboratories (Sulzfeld, Germany). Intracranial tumor cell implantation has been previously described(101). The animal experiments were carried out under the project license ZH04/2018 (subcutaneous tumor models) and ZH73/2018 (glioblastoma) granted by the Veterinäramt des Kantons Zürich, Switzerland, in compliance with the Swiss Animal Protection Act (TSchG) and the Swiss Animal Protection Ordinance (TSchV).

Cloning

A soluble single-chain trimer of murine 4-1BBL was designed by linking the TNF homology domain (amino acids 139 – 309) with a single glycine as a linker. The genetic sequence was ordered from Eurofins Genomics. The sequence was then introduced into a vector encoding the F8 in a diabody format by Gibson Isothermal Assembly. To clone the single-chain variable Fragment (scFv) linked to the 4-1BBL monomer, the genetic sequence encoding the diabody was replaced by the sequence encoding the scFv and two domains of 4-1BBL were removed by PCR followed by blunt-end ligation. Additional base pairs of 4-1BBL were added to the 4-1BBL sequence by PCR followed by blunt-end ligation. The IgG fusion proteins were cloned by fusing the 4-1BBL sequence to the sequence of the antibody in the IgG format by PCR before introducing it into an appropriate vector by restriction cloning. The protein sequences are provided in [**Supplementary Table S1**].

Protein production

Proteins were produced by transient transfection of CHO-S cells and purified by protein A affinity chromatography as described previously (68, 103, 104). Quality control of the purified products included SDS-PAGE and size exclusion chromatography using an Äkta Pure FPLC system (GE Healthcare) with a Superdex S200 10/300 increase column at a flow rate of 0.75 mL/min (GE Healthcare) [**Figure 1 and Supplementary Figure S1**].

Binding measurements by Surface Plasmon Resonance

To evaluate the binding kinetics of the F8 antibody fragment to EDA, a CM5 sensor chip (GE Healthcare) was coated with approximately 500 resonance units of an EDA-containing recombinant fragment of fibronectin. The measurements were carried out with a Biacore S200 (GE Healthcare). The contact time was set to 3 min at a flow rate of 20 μL/min followed by a dissociation for 10 min and a regeneration of the chip using 10 mM HCl.

Binding measurements by Flow Cytometry

In order to measure the binding of the 4-1BBL moiety to cells expressing 4-1BB, CTLL-2 cells were incubated with varying concentrations of the fusion proteins for 1 h. The bound protein was detected by addition of an excess of AlexaFluor488-labelled protein A (Thermofisher, #P11047) and subsequent measurement of the fluorescence using a Cytoflex Flow Cytometer. The mean fluorescence was normalized and the resulting binding curve was fitted using the the [Agonist] vs. response (three parameters) fit of the GraphPad Prism 7.0 a software to estimate the functional K_D.

NF-κB response assay

The development of the CTLL-2 reporter cell line is described elsewhere(66). CTLL-2_NF-κB reporter cells were starved by washing the cells twice with prewarmed HBSS (Gibco, #14175095) followed by growth in the absence of IL-2 for 6 - 9 h in RPMI 1640 (Gibco, # 21875034) medium supplemented with 10% FBS (Gibco, #10270106), 1 X antibiotic-antimycoticum (Gibco, # 15240062), 2 mM Ultraglutamine (Lonza, # BE17-605E/U1), 25 mM HEPES (Gibco, # 15630080) and 50 μM β-mercaptoethanol (Sigma Aldrich) in order to reduce the background signal. To coat the wells with antigen, 100 μL 100 nM 11-A-12 fibronectin in phosphate buffered saline (PBS) was added to each well and the plate was incubated at 37°C for 90 min. Cells were seeded in 96-well plates (50,000 cells/well) and growth medium containing varying concentrations of the antibody-cytokine conjugate was added. The cells were incubated at 37°C, 5% CO_2 for several hours. To assess luciferase production, 20 μL of the supernatant was transferred to an opaque 96-well plate (PerkinElmer, Optiplate-96, white, #6005290) and 80 μL 1 μg/mL Coelenterazine (Carl Roth AG, #4094.3) in phosphate buffered saline (PBS) was added. Luminescence at 595 nm was measured immediately. The relative luminescence was calculated by dividing the obtained results by the results obtained when no inducer was added. The data was fitted using the [Agonist] vs. response (three parameters) fit of the GraphPad Prism 7.0 a software to estimate the EC_{50}.

Quantitative biodistribution studies

Quantitative biodistribution experiments were carried out as described previously(44). Briefly, 8 weeks old female 129/Sv mice were injected subcutaneously in the right flank with 10^7 F9 teratocarcinoma cells. The tumor size was measured daily with a caliper and the volume was calculated using the formula [volume = length x width x width x 0.5]. When the tumors reached a volume of 100 – 300 mm^3, 10 μg of radioiodinated protein was injected into the lateral tail vein. The mice were sacrificed 24 h after the injection and the organs were excised and weighed. The radioactivity of the different organs was measured (Packard Cobra II Gamma Counter) and expressed as percentage of injected dose per gram of tissue (%ID/g ± SD, $n = 3$).

***Ex vivo* detection of fluorescently labelled immunocytokines**

For fluorescent labelling, the proteins were resuspended in a 0.1 M sodium carbonate buffer at pH 9.1 and an excess of Fluorescein Isothiocyanate (FITC) was added. The reaction was carried out overnight at 4°C. The labelled proteins were separated from unconjugated FITC by PD-10. Approximately 100 μg of fluorescently-labelled protein was injected into the lateral tail-vein of tumor-bearing mice. The mice were sacrificed 24 h after the injection. The organs were excised

and embedded in NEG-50 cryoembedding medium (ThermoFisher, Richard-Allan-Scientific, #6502) prior to freezing. For staining, 8 µm cryosections were fixed in acetone and incubated with goat-anti-mouse CD31 (R&D system, #AF3628, 1:200) and rabbit-anti-FITC (Biorad, #4510-7804) followed by donkey-anti-goat-AF594 (Invitrogen, #A11058) and donkey-anti-rabbit-AF488 (Invitrogen, #A21206). Images were acquired using a Zeiss Axioscope 2 mot plus with an Axiocam 503 camera at a 200 X magnification in the RGB mode. The images were processed using the software ImageJ v1.52k setting the thresholds for the red channel to 14-80 and the green channel to 15 - 100.

~~**Immunofluorescence on tissue microarray**~~

~~Immunofluorescence was performed onto Frozen Tumor and Normal Tissue Array (Biochain, #T6235700). The array was fixed by ice-cold aceton for 5 minutes. After fixation, sections were let dry at room temperature for 10 minutes and then blocked for 45 min with 20% fetal bovine serum in PBS. FITC labeled IgG(F8) was added at 5 µg/ml in 2% BSA/PBS solution for 1h at room temperature. The tissue array was then washed twice with PBS and secondary rabbit anti-FITC antibody (Biorad, #4510-7804) was added to a final 1:1000 dilution in 2% BSA/PBS at room temperature for 1h. After washing the array twice with PBS, Goat Anti-Rabbit Alexa-488 (ThermoFisher, #A11032) was added to a final 1:500 dilution in 2% BSA/PBS. Dapi was used to counterstain nuclei. Slides were analyzed with Axioskop2 plus microscope (Zeiss).~~

Therapy studies in subcutaneous tumor models

After the subcutaneous implantation of the tumor cells into the right flank of 8 weeks old female mice, the tumor size was monitored by caliper measurements on a daily basis [volume = length x width x width x 0.5]. In the preventive setting, the therapy was started when the tumor reached a volume of 40 mm^3 and for the therapeutic setting, the therapy was started when the tumors reached a volume of 75 – 100 mm^3. The mice were grouped in order to obtain groups of similar average tumor size (n = 5-6). The mice either received 100 µL Saline (PBS, Gibco, #1010023), 500 µg F8(scFv)-4-1BBL, 200 µg αPD-1 (BioXCell, clone 29F.1A12) or a combination of the checkpoint inhibitor and the immunocytokine. For the combination treatment, the checkpoint inhibitor was administered one day prior to the immunocytokine. The therapeutic agents were administrated every second day in a total of three cycles intravenously into the lateral tail vein. The animals were sacrificed if the tumor diameter exceeded 15 mm or when the tumor started to ulcerate. Some cured mice were rechallenged by the subcutaneous injection of WEHI 164 or CT26 tumor cells after being tumor-free for at least 4 weeks. Statistical evaluations were done using a standard two-way ANOVA followed by the Tukey's multiple comparison test with GraphPad Prism v8.4.1.

Magnetic resonance imaging and glioblastoma studies

Coronal T2-weighted MRI images at day 12 after tumor implantation were acquired using Paravision 6.0 (Bruker BioSpin) on a 4.7 T small animal magnetic resonance imager (Pharmascan; Bruker Biospin, Ettlingen, Germany). Mean ± SD of the tumor perimeter in mm at the maximum circumference were determined using the Medical Image Processing, Analysis, and Visualization (MIPAV) software (https://mipav.cit.nih.gov/). Mice were sacrificed when developing neurologic symptoms. Kaplan Meier survival analysis was performed to assess survival differences among the treatment groups and p values were calculated with Gehan-Breslow-Wilcoxon test using GraphPad Prism v7.0 a. Significance was tested at *$p < 0.05$ and **$p < 0.01$.

Analysis of tumor-infiltrating lymphocytes by flow cytometry

The mice were sacrificed 48 h after the second therapy cycle. The tumor-draining lymph nodes as well as the tumor were excised. A single-cell suspension of the tumor was obtained by digesting it in RPMI 1640 supplemented with 1 mg/mL collagenase II and 100 µg/mL DNase I for 30 min at 37°C. After the digestion, the suspension was passed through a 70 µm cell strainer. If necessary, the red blood cells were removed using a red blood cell lysis buffer (Roche). The lymph nodes were smashed on a 70 µm cell strainer and washed with PBS. For cell surface staining, cells were incubated with a mix of suitable antibodies: αCD3-APC/Cy7 (Biolegend, #100222), αCD4-APC (Biolegend, #100412), αCD8-FITC (Biolegend, #100706), αNK1.1-PE (Biolegend, #108708), αCD62L-BV421 (Biolegend, #104436), αCD44-APC/Cy7 (Biolegend, #103028), αMHCII(IA/IE)-BV421 (Biolegend, #107631), αPD-1-BV421 (Biolegend, #109121) and αCD39-APC (Biolegend, #143809). After staining of the cell surface markers, the cells were stained with 7-AAD (Biolegend) for live/dead discrimination. For intracellular staining, the cells were first stained with Zombie Red (SigmaAldrich) and then the cell surface stain was performed. The cells were fixed and permeabilized using the eBioscience™ FoxP3/Transcription Factor Staining Buffer Set (Thermofisher, #00-5523-00) according to the manufacturer's instructions. The fluorescence was measured using a Cytoflex Flow Cytometer and the data was evaluated using the FlowJo software. The gating strategy is depicted in [**Supplementary Figure S8**]. Statistical evaluations were done using a regular two-way ANOVA followed by a Tukey's multiple comparison test or a regular one-way ANOVA followed by a Sidak's multiple comparison test in GraphPad Prism v8.4.1.

Acknowledgments

Financial support from the ETH Zürich, the Swiss National Science Foundation (grant number 310030_182003/1) and the European Research Council (ERC) under the European Union's Horizon 2020 research and innovation program (grant agreement 670603) is gratefully acknowledged. The authors gratefully acknowledge the support of the Scientific Center for Optical and Electron Microscopy (ScopeM) of the ETH Zurich. In addition, Sabrina Müller and Fiona Amman are gratefully acknowledged for their technical assistance especially for the protein production. The authors would also like to thank Lisa Nadal for her help with some immunofluorescence stainings.

References

1. Lee S & Margolin K (2011) Cytokines in cancer immunotherapy. *Cancers (Basel)* 3(4):3856-3893.
2. Murer P & Neri D (2019) Antibody-cytokine fusion proteins: A novel class of biopharmaceuticals for the therapy of cancer and of chronic inflammation. *N Biotechnol* 52:42-53.
3. Dranoff G (2004) Cytokines in cancer pathogenesis and cancer therapy. *Nat Rev Cancer* 4(1):11-22.
4. Parmiani G, Rivoltini L, Andreola G, & Carrabba M (2000) Cytokines in cancer therapy. *Immunol Lett* 74(1):41-44.
5. Zappasodi R, Merghoub T, & Wolchok JD (2018) Emerging Concepts for Immune Checkpoint Blockade-Based Combination Therapies. *Cancer Cell* 34(4):690.
6. Hutmacher C, Gonzalo Nunez N, Liuzzi AR, Becher B, & Neri D (2019) Targeted Delivery of IL2 to the Tumor Stroma Potentiates the Action of Immune Checkpoint Inhibitors by Preferential Activation of NK and CD8(+) T Cells. *Cancer Immunol Res* 7(4):572-583.
7. Vacchelli E*, et al.* (2016) Trial Watch-Immunostimulation with cytokines in cancer therapy. *Oncoimmunology* 5(2):e1115942.
8. Rosenberg SA (2014) IL-2: the first effective immunotherapy for human cancer. *J Immunol* 192(12):5451-5458.
9. Atkins MB*, et al.* (1999) High-dose recombinant interleukin 2 therapy for patients with metastatic melanoma: analysis of 270 patients treated between 1985 and 1993. *J Clin Oncol* 17(7):2105-2116.
10. Adams VR & Brenner T (1999) Oprelvekin (Neumega), first platelet growth factor for thrombocytopenia. *J Am Pharm Assoc (Wash)* 39(5):706-707.

11. Wilde MI & Faulds D (1998) Oprelvekin: a review of its pharmacology and therapeutic potential in chemotherapy-induced thrombocytopenia. *BioDrugs* 10(2):159-171.
12. Chapman PB*, et al.* (1987) Clinical pharmacology of recombinant human tumor necrosis factor in patients with advanced cancer. *J Clin Oncol* 5(12):1942-1951.
13. Taguchi T (1986) Clinical studies of recombinant interferon alfa-2a (Roferon-A) in cancer patients. *Cancer* 57(8 Suppl):1705-1708.
14. Spiegel RJ (1985) INTRON A (interferon alfa-2b): clinical overview. *Cancer Treat Rev* 12 Suppl B:5-16.
15. Limmroth V, Putzki N, & Kachuck NJ (2011) The interferon beta therapies for treatment of relapsing-remitting multiple sclerosis: are they equally efficacious? A comparative review of open-label studies evaluating the efficacy, safety, or dosing of different interferon beta formulations alone or in combination. *Ther Adv Neurol Disord* 4(5):281-296.
16. Madsen C (2017) The innovative development in interferon beta treatments of relapsing-remitting multiple sclerosis. *Brain Behav* 7(6):e00696.
17. Miller CH, Maher SG, & Young HA (2009) Clinical Use of Interferon-gamma. *Ann N Y Acad Sci* 1182:69-79.
18. Herman AC, Boone TC, & Lu HS (1996) Characterization, formulation, and stability of Neupogen (Filgrastim), a recombinant human granulocyte-colony stimulating factor. *Pharm Biotechnol* 9:303-328.
19. Geigert J & Ghrist FD (1996) Development and shelf-life determination of recombinant human granulocyte--macrophage colony-stimulating factor (LEUKINE, GM-CSF). *Pharm Biotechnol* 9:329-342.
20. Vazquez E (1999) Leukine studies move forward. *Posit Aware* 10(4):29.
21. Lejeune F*, et al.* (1995) Administration of high-dose tumor necrosis factor alpha by isolation perfusion of the limbs. Rationale and results. *J Infus Chemother* 5(2):73-81.

22. Leonard JP*, et al.* (1997) Effects of single-dose interleukin-12 exposure on interleukin-12-associated toxicity and interferon-gamma production. *Blood* 90(7):2541-2548.
23. Geertsen PF, Gore ME, Negrier S, Tourani JM, & von der Maase H (2004) Safety and efficacy of subcutaneous and continuous intravenous infusion rIL-2 in patients with metastatic renal cell carcinoma. *Br J Cancer* 90(6):1156-1162.
24. Baldo BA (2014) Side effects of cytokines approved for therapy. *Drug Saf* 37(11):921-943.
25. Eliason JF (2001) Pegylated cytokines: potential application in immunotherapy of cancer. *BioDrugs* 15(11):705-711.
26. Jazayeri JA & Carroll GJ (2008) Fc-based cytokines : prospects for engineering superior therapeutics. *BioDrugs* 22(1):11-26.
27. Charych DH*, et al.* (2016) NKTR-214, an Engineered Cytokine with Biased IL2 Receptor Binding, Increased Tumor Exposure, and Marked Efficacy in Mouse Tumor Models. *Clin Cancer Res* 22(3):680-690.
28. Harvill ET & Morrison SL (1995) An IgG3-IL2 fusion protein activates complement, binds Fc gamma RI, generates LAK activity and shows enhanced binding to the high affinity IL-2R. *Immunotechnology* 1(2):95-105.
29. Lode HN, Xiang R, Becker JC, Gillies SD, & Reisfeld RA (1998) Immunocytokines: a promising approach to cancer immunotherapy. *Pharmacol Ther* 80(3):277-292.
30. Hu P*, et al.* (1996) A chimeric Lym-1/interleukin 2 fusion protein for increasing tumor vascular permeability and enhancing antibody uptake. *Cancer Res* 56(21):4998-5004.
31. Sharifi J, Khawli LA, Hu P, Li J, & Epstein AL (2002) Generation of human interferon gamma and tumor Necrosis factor alpha chimeric TNT-3 fusion proteins. *Hybrid Hybridomics* 21(6):421-432.
32. Penichet ML & Morrison SL (2001) Antibody-cytokine fusion proteins for the therapy of cancer. *J Immunol Methods* 248(1-2):91-101.

33. Young PA, Morrison SL, & Timmerman JM (2014) Antibody-cytokine fusion proteins for treatment of cancer: engineering cytokines for improved efficacy and safety. *Semin Oncol* 41(5):623-636.
34. Halin C*, et al.* (2002) Enhancement of the antitumor activity of interleukin-12 by targeted delivery to neovasculature. *Nat Biotechnol* 20(3):264-269.
35. Lechner MG, Russell SM, Bass RS, & Epstein AL (2011) Chemokines, costimulatory molecules and fusion proteins for the immunotherapy of solid tumors. *Immunotherapy* 3(11):1317-1340.
36. Sondel PM & Gillies SD (2012) Current and Potential Uses of Immunocytokines as Cancer Immunotherapy. *Antibodies (Basel)* 1(2):149-171.
37. Kontermann RE (2012) Antibody-cytokine fusion proteins. *Arch Biochem Biophys* 526(2):194-205.
38. Fyfe G*, et al.* (1995) Results of treatment of 255 patients with metastatic renal cell carcinoma who received high-dose recombinant interleukin-2 therapy. *J Clin Oncol* 13(3):688-696.
39. Johannsen M*, et al.* (2010) The tumour-targeting human L19-IL2 immunocytokine: preclinical safety studies, phase I clinical trial in patients with solid tumours and expansion into patients with advanced renal cell carcinoma. *Eur J Cancer* 46(16):2926-2935.
40. Eigentler TK*, et al.* (2011) A dose-escalation and signal-generating study of the immunocytokine L19-IL2 in combination with dacarbazine for the therapy of patients with metastatic melanoma. *Clin Cancer Res* 17(24):7732-7742.
41. Spitaleri G*, et al.* (2013) Phase I/II study of the tumour-targeting human monoclonal antibody-cytokine fusion protein L19-TNF in patients with advanced solid tumours. *J Cancer Res Clin Oncol* 139(3):447-455.
42. Strauss J*, et al.* (2019) First-in-Human Phase I Trial of a Tumor-Targeted Cytokine (NHS-IL12) in Subjects with Metastatic Solid Tumors. *Clin Cancer Res* 25(1):99-109.

43. Puca E, De Luca R, Seehusen F, Rodriguez JMM, & Neri D (2020) Comparative evaluation of bolus and fractionated administration modalities for two antibody-cytokine fusions in immunocompetent tumor-bearing mice. *J Control Release* 317:282-290.

44. Villa A*, et al.* (2008) A high-affinity human monoclonal antibody specific to the alternatively spliced EDA domain of fibronectin efficiently targets tumor neo-vasculature in vivo. *Int J Cancer* 122(11):2405-2413.

45. Rybak JN, Roesli C, Kaspar M, Villa A, & Neri D (2007) The extra-domain A of fibronectin is a vascular marker of solid tumors and metastases. *Cancer Res* 67(22):10948-10957.

46. White ES, Baralle FE, & Muro AF (2008) New insights into form and function of fibronectin splice variants. *J Pathol* 216(1):1-14.

47. Schwager K*, et al.* (2011) A comparative immunofluorescence analysis of three clinical-stage antibodies in head and neck cancer. *Head Neck Oncol* 3:25.

48. Schwager K*, et al.* (2009) Preclinical characterization of DEKAVIL (F8-IL10), a novel clinical-stage immunocytokine which inhibits the progression of collagen-induced arthritis. *Arthritis Res Ther* 11(5):R142.

49. Goodwin RG*, et al.* (1993) Molecular cloning of a ligand for the inducible T cell gene 4-1BB: a member of an emerging family of cytokines with homology to tumor necrosis factor. *Eur J Immunol* 23(10):2631-2641.

50. Pollok KE*, et al.* (1994) 4-1BB T-cell antigen binds to mature B cells and macrophages, and costimulates anti-mu-primed splenic B cells. *Eur J Immunol* 24(2):367-374.

51. DeBenedette MA*, et al.* (1999) Analysis of 4-1BB ligand (4-1BBL)-deficient mice and of mice lacking both 4-1BBL and CD28 reveals a role for 4-1BBL in skin allograft rejection and in the cytotoxic T cell response to influenza virus. *J Immunol* 163(9):4833-4841.

52. Pollok KE*, et al.* (1993) Inducible T cell antigen 4-1BB. Analysis of expression and function. *J Immunol* 150(3):771-781.
53. Melero I, Johnston JV, Shufford WW, Mittler RS, & Chen L (1998) NK1.1 cells express 4-1BB (CDw137) costimulatory molecule and are required for tumor immunity elicited by anti-4-1BB monoclonal antibodies. *Cell Immunol* 190(2):167-172.
54. McHugh RS*, et al.* (2002) CD4(+)CD25(+) immunoregulatory T cells: gene expression analysis reveals a functional role for the glucocorticoid-induced TNF receptor. *Immunity* 16(2):311-323.
55. Makkouk A, Chester C, & Kohrt HE (2016) Rationale for anti-CD137 cancer immunotherapy. *Eur J Cancer* 54:112-119.
56. Menk AV*, et al.* (2018) 4-1BB costimulation induces T cell mitochondrial function and biogenesis enabling cancer immunotherapeutic responses. *The Journal of experimental medicine* 215(4):1091-1100.
57. Bitra A, Doukov T, Croft M, & Zajonc DM (2018) Crystal structures of the human 4-1BB receptor bound to its ligand 4-1BBL reveal covalent receptor dimerization as a potential signaling amplifier. *J Biol Chem* 293(26):9958-9969.
58. Bitra A*, et al.* (2018) Crystal structure of murine 4-1BB and its interaction with 4-1BBL support a role for galectin-9 in 4-1BB signaling. *J Biol Chem* 293(4):1317-1329.
59. Bitra A, Doukov T, Destito G, Croft M, & Zajonc DM (2019) Crystal structure of the m4-1BB/4-1BBL complex reveals an unusual dimeric ligand that undergoes structural changes upon 4-1BB receptor binding. *J Biol Chem* 294(6):1831-1845.
60. Fellermeier S*, et al.* (2016) Advancing targeted co-stimulation with antibody-fusion proteins by introducing TNF superfamily members in a single-chain format. *Oncoimmunology* 5(11):e1238540.

61. Huston JS*, et al.* (1988) Protein engineering of antibody binding sites: recovery of specific activity in an anti-digoxin single-chain Fv analogue produced in Escherichia coli. *Proc Natl Acad Sci U S A* 85(16):5879-5883.
62. Bird RE*, et al.* (1988) Single-chain antigen-binding proteins. *Science* 242(4877):423-426.
63. Holliger P, Prospero T, & Winter G (1993) "Diabodies": small bivalent and bispecific antibody fragments. *Proc Natl Acad Sci U S A* 90(14):6444-6448.
64. Hutmacher C & Neri D (2018) Antibody-cytokine fusion proteins: Biopharmaceuticals with immunomodulatory properties for cancer therapy. *Adv Drug Deliv Rev*.
65. Bootz F & Neri D (2016) Immunocytokines: a novel class of products for the treatment of chronic inflammation and autoimmune conditions. *Drug Discov Today* 21(1):180-189.
66. Mock J, Pellegrino C, & Neri D (2020) A universal reporter cell line for bioactivity evaluation of engineered cytokine products. *Sci Rep* 10(1):3234.
67. Frey K, Zivanovic A, Schwager K, & Neri D (2011) Antibody-based targeting of interferon-alpha to the tumor neovasculature: a critical evaluation. *Integr Biol (Camb)* 3(4):468-478.
68. Hemmerle T*, et al.* (2013) The antibody-based targeted delivery of TNF in combination with doxorubicin eradicates sarcomas in mice and confers protective immunity. *Br J Cancer* 109(5):1206-1213.
69. Probst P*, et al.* (2017) Sarcoma Eradication by Doxorubicin and Targeted TNF Relies upon CD8(+) T-cell Recognition of a Retroviral Antigen. *Cancer Res* 77(13):3644-3654.
70. Mosely SI*, et al.* (2017) Rational Selection of Syngeneic Preclinical Tumor Models for Immunotherapeutic Drug Discovery. *Cancer Immunol Res* 5(1):29-41.

71. Yu JW*, et al.* (2018) Tumor-immune profiling of murine syngeneic tumor models as a framework to guide mechanistic studies and predict therapy response in distinct tumor microenvironments. *PLoS One* 13(11):e0206223.
72. Selby MJ*, et al.* (2016) Preclinical Development of Ipilimumab and Nivolumab Combination Immunotherapy: Mouse Tumor Models, In Vitro Functional Studies, and Cynomolgus Macaque Toxicology. *PLoS One* 11(9):e0161779.
73. Huang AY*, et al.* (1996) The immunodominant major histocompatibility complex class I-restricted antigen of a murine colon tumor derives from an endogenous retroviral gene product. *Proc Natl Acad Sci U S A* 93(18):9730-9735.
74. Puca E*, et al.* (2020) The antibody-based delivery of interleukin-12 to solid tumors boosts NK and CD8(+) T cell activity and synergizes with immune checkpoint inhibitors. *Int J Cancer* 146(9):2518-2530.
75. Scott AC*, et al.* (2019) TOX is a critical regulator of tumour-specific T cell differentiation. *Nature* 571(7764):270-274.
76. Canale FP*, et al.* (2018) CD39 Expression Defines Cell Exhaustion in Tumor-Infiltrating CD8(+) T Cells. *Cancer Res* 78(1):115-128.
77. Chester C, Ambulkar S, & Kohrt HE (2016) 4-1BB agonism: adding the accelerator to cancer immunotherapy. *Cancer Immunol Immunother* 65(10):1243-1248.
78. Dubrot J*, et al.* (2010) Treatment with anti-CD137 mAbs causes intense accumulations of liver T cells without selective antitumor immunotherapeutic effects in this organ. *Cancer Immunol Immunother* 59(8):1223-1233.
79. Bartkowiak T*, et al.* (2018) Activation of 4-1BB on Liver Myeloid Cells Triggers Hepatitis via an Interleukin-27-Dependent Pathway. *Clin Cancer Res* 24(5):1138-1151.
80. Qi X*, et al.* (2019) Optimization of 4-1BB antibody for cancer immunotherapy by balancing agonistic strength with FcgammaR affinity. *Nat Commun* 10(1):2141.

81. Ho SK, *et al.* (2020) Epitope and Fc-Mediated Cross-linking, but Not High Affinity, Are Critical for Antitumor Activity of CD137 Agonist Antibody with Reduced Liver Toxicity. *Mol Cancer Ther* 19(4):1040-1051.
82. Compte M, *et al.* (2018) A tumor-targeted trimeric 4-1BB-agonistic antibody induces potent anti-tumor immunity without systemic toxicity. *Nat Commun* 9(1):4809.
83. Mikkelsen K, *et al.* (2019) Carcinoembryonic Antigen (CEA)-Specific 4-1BB-Costimulation Induced by CEA-Targeted 4-1BB-Agonistic Trimerbodies. *Front Immunol* 10:1791.
84. Claus C, *et al.* (2019) Tumor-targeted 4-1BB agonists for combination with T cell bispecific antibodies as off-the-shelf therapy. *Sci Transl Med* 11(496).
85. Hinner MJ, *et al.* (2019) Tumor-Localized Costimulatory T-Cell Engagement by the 4-1BB/HER2 Bispecific Antibody-Anticalin Fusion PRS-343. *Clin Cancer Res* 25(19):5878-5889.
86. Neri D (2019) Antibody-Cytokine Fusions: Versatile Products for the Modulation of Anticancer Immunity. *Cancer Immunol Res* 7(3):348-354.
87. Gillies SD (2013) A new platform for constructing antibody-cytokine fusion proteins (immunocytokines) with improved biological properties and adaptable cytokine activity. *Protein Eng Des Sel* 26(10):561-569.
88. Wuest T, *et al.* (2002) TNF-Selectokine: a novel prodrug generated for tumor targeting and site-specific activation of tumor necrosis factor. *Oncogene* 21(27):4257-4265.
89. Huyghe L, *et al.* (2020) Safe eradication of large established tumors using neovasculature-targeted tumor necrosis factor-based therapies. *EMBO Mol Med* 12(2):e11223.
90. Cauwels A, *et al.* (2018) A safe and highly efficient tumor-targeted type I interferon immunotherapy depends on the tumor microenvironment. *Oncoimmunology* 7(3):e1398876.

91. Pogue SL*, et al.* (2016) Targeting Attenuated Interferon-alpha to Myeloma Cells with a CD38 Antibody Induces Potent Tumor Regression with Reduced Off-Target Activity. *PLoS One* 11(9):e0162472.
92. Venetz D, Koovely D, Weder B, & Neri D (2016) Targeted Reconstitution of Cytokine Activity upon Antigen Binding using Split Cytokine Antibody Fusion Proteins. *J Biol Chem* 291(35):18139-18147.
93. Bodmer JL, Schneider P, & Tschopp J (2002) The molecular architecture of the TNF superfamily. *Trends Biochem Sci* 27(1):19-26.
94. Labrijn AF, Janmaat ML, Reichert JM, & Parren P (2019) Bispecific antibodies: a mechanistic review of the pipeline. *Nat Rev Drug Discov* 18(8):585-608.
95. Dahlen E, Veitonmaki N, & Norlen P (2018) Bispecific antibodies in cancer immunotherapy. *Ther Adv Vaccines Immunother* 6(1):3-17.
96. Reichen C*, et al.* (2018) FAP-mediated tumor accumulation of a T-cell agonistic FAP/4-1BB DARPin drug candidate analyzed by SPECT/CT and quantitative biodistribution. (AACR).
97. Hurov K*, et al.* (2019) A novel fully synthetic dual targeted Nectin-4/4-1BB Bicycle (R) peptide induces tumor localized 4-1BB agonism. *Journal for Immunotherapy of Cancer* 7.
98. Muller J, Baeyens A, & Dustin ML (2018) Tumor Necrosis Factor Receptor Superfamily in T Cell Priming and Effector Function. *Adv Immunol* 140:21-57.
99. Li J, Yin Q, & Wu H (2013) Structural basis of signal transduction in the TNF receptor superfamily. *Adv Immunol* 119:135-153.
100. Vanamee ES & Faustman DL (2018) Structural principles of tumor necrosis factor superfamily signaling. *Sci Signal* 11(511).
101. Weiss T*, et al.* (2018) NKG2D-Dependent Antitumor Effects of Chemotherapy and Radiotherapy against Glioblastoma. *Clin Cancer Res* 24(4):882-895.

102. Weiss T, Weller M, Guckenberger M, Sentman CL, & Roth P (2018) NKG2D-Based CAR T Cells and Radiotherapy Exert Synergistic Efficacy in Glioblastoma. *Cancer Res* 78(4):1031-1043.

103. Carnemolla B*, et al.* (2002) Enhancement of the antitumor properties of interleukin-2 by its targeted delivery to the tumor blood vessel extracellular matrix. *Blood* 99(5):1659-1665.

104. Pasche N, Wulhfard S, Pretto F, Carugati E, & Neri D (2012) The antibody-based delivery of interleukin-12 to the tumor neovasculature eradicates murine models of cancer in combination with paclitaxel. *Clin Cancer Res* 18(15):4092-4103.

Figures and Tables

Figure 1. The nine F8-4-1BBL fusion proteins that were designed and tested in this study **(a)** schematic depiction of an antibody in the IgG format and of the human 4-1BBL. The human 4-1BBL is a transmembrane protein which forms a non-covalent homotrimer(57) **(b)** the fusion proteins featuring murine 4-1BBL are schematically depicted and size exclusion chromatograms are provided.

Figure 2. *In vitro* characterization of five F8-4-1BBL formats **(a)** binding to 4-1BB was measured by flow cytometry with the murine cytotoxic T cell line CTLL-2 which expresses 4-1BB **(b)** binding of the F8 moiety to the EDA-positive ectodomain of fibronectin was measured by surface plasmon resonance on chips coated with recombinant EDA **(c)** biological activity was tested using an NF-κB reporter cell line that secretes luciferase upon activation of the NF-κB pathway by signaling through 4-1BB. The assay was performed both with and without EDA immobilized on solid support ($n = 3$). Curve fitting was done using the [agonist] vs response (three parameters) fit of GraphPad Prism v7.0. Data represent mean ± SD.

Figure 3. *In vivo* biodistribution studies of three F8-4-1BBL formats **(a)** The mice were sacrificed 24 h after the injection of the radioiodinated proteins and the radioactivity of excised organs was measured and expressed as percent injected dose per gram of tissue (%ID/g ± SD, *n* = 3). The KSF antibody targeting hen egg lysozyme was used as untargeted control(67). **(b)** The mice were sacrificed 24 h after the injection of FITC-labelled F8-4-1-BBL or KSF-4-1-BBL in format **5**. The proteins were detected *ex vivo* on cryosections (green: αFITC, red: αCD31). ~~**(c)** The expression of EDA was assessed on human tissue microarrays using FITC-labelled F8 in the IgG format. (green: EDA, blue: nuclei).~~

Figure 4. Therapy studies with F8-4-1BBL in format **5 (a)** The preventive therapy in WEHI-164 fibrosarcoma-bearing mice was started on day 5 when the tumors reached a volume of 40 mm^3. The tumor sizes are shown as mean + SD (*n* = 5). The body weight data is represented as mean body weight change ± SD for each group. **(b)** The therapy in WEHI-164 fibrosarcoma-bearing mice was started on day 7 when the tumor volume was > 80mm^3. The tumor sizes are shown as mean + SD (*n* = 5). The statistical results of a regular two-way ANOVA followed by a Tukey's multiple comparison test using GraphPad Prism v8.4.1 on day 13 are shown (ns: not significant, * p = 0.0427). The body weight data is represented as mean body weight change ± SD for each group. **(c)** In CT26-colon carcinoma-bearing mice the therapy was started on day 7 when the tumor volume exceeded 80 mm^3. The tumor sizes are shown as mean + SD (*n* = 5). The result of a regular two-way ANOVA followed by a Tukey's multiple comparison test using GraphPad Prism v8.4.1 revealed that as of day 13 the tumor size of the mice treated with PD-1 blockade was significantly smaller than the size of the tumors treated with saline (*** p = 0.0004). **(d)** In MC-38 colon carcinoma-bearing mice the therapy was started on day 7 when the tumor volume exceeded 75 mm^3. The tumor sizes are shown as mean + SD (*n* = 5 - 6). The result of a regular two-way ANOVA followed by a Tukey's multiple comparison test using GraphPad Prism v8.4.1 is shown for day 12 (*** p < 0.001). The body weight data is represented as mean body weight change ± SD for each group. **(e)** GL-261 were implanted orthotopically in C57BL/6 mice. Subsequently, mice were treated intravenously with saline, F8-4-1BBL, αPD-1 or the combination starting on day 5. Tumor size was assessed at day 12 after tumor implantation. MRI of five mice per group are shown on the left with tumors outlined in red and the quantification of tumor perimeters in 5 mice per group on the right. The survival data are presented as Kaplan-Meier plots (*n* = 5). Results from a Gehan-Breslow-Wilcoxon test revealed significant (p = 0.0036) differences between the survival curves of the different treatment groups. The body weight data is represented as mean body weight change ± SD for each group. (black arrows: injections of the single-agents, grey arrows: injection of F8-4-1BBL in the combination treatment, CR: complete response)

Figure 5. Analysis of tumor-infiltrating leukocytes (TIL) and tumor-draining lymph nodes (TDLN) **(a)** Composition of the tumor-infiltrating immune cells, including the CD8:CD4 ratio, the proportion of AH1-specific CD8+ T cells and regulatory CD4+ T cells in WEHI-164 and CT26 tumors treated with saline, F8-4-1BBL and the combo therapy (αPD-1 and F8-4-1BBL). Proportion of AH1-specific CD8+ T cells and regulatory CD4+ T cell are shown also for matching TDLNs**. (b)** Composition of the TDLNs in WEHI-164 and CT26 tumor-bearing mice, including the CD8:CD4 ratio **(c)** Phenotype of the CD8+ T cells and AH1-specific CD8+ T cells in CD26 tumor-bearing mice from different treatment groups. The phenotype was assessed based on the expression of CD62L, CD44 and the exhaustion markers CD39 and PD-1. The data represents individual values, means and standard deviations. Statistical evaluations were performed using a regular two-way ANOVA followed by a Tukey's multiple comparison test using GraphPad Prism v8.4.1 [* $p < 0.05$, ** $p < 0.01$, *** $p < 0.001$, **** $p < 0.0001$] (TIL: tumor-infiltrating leukocyte, NKT: natural killer T cell, NK: natural killer cell, APC: antigen-presenting cell, T_{reg}: regulatory T cell, TDLN: tumor-draining lymph node, Teff: effector T cell [CD44+CD62L-], Tcm: central memory T cell [CD44+CD62L+], Tnaive: naïve T cell [CD44-CD62L+])

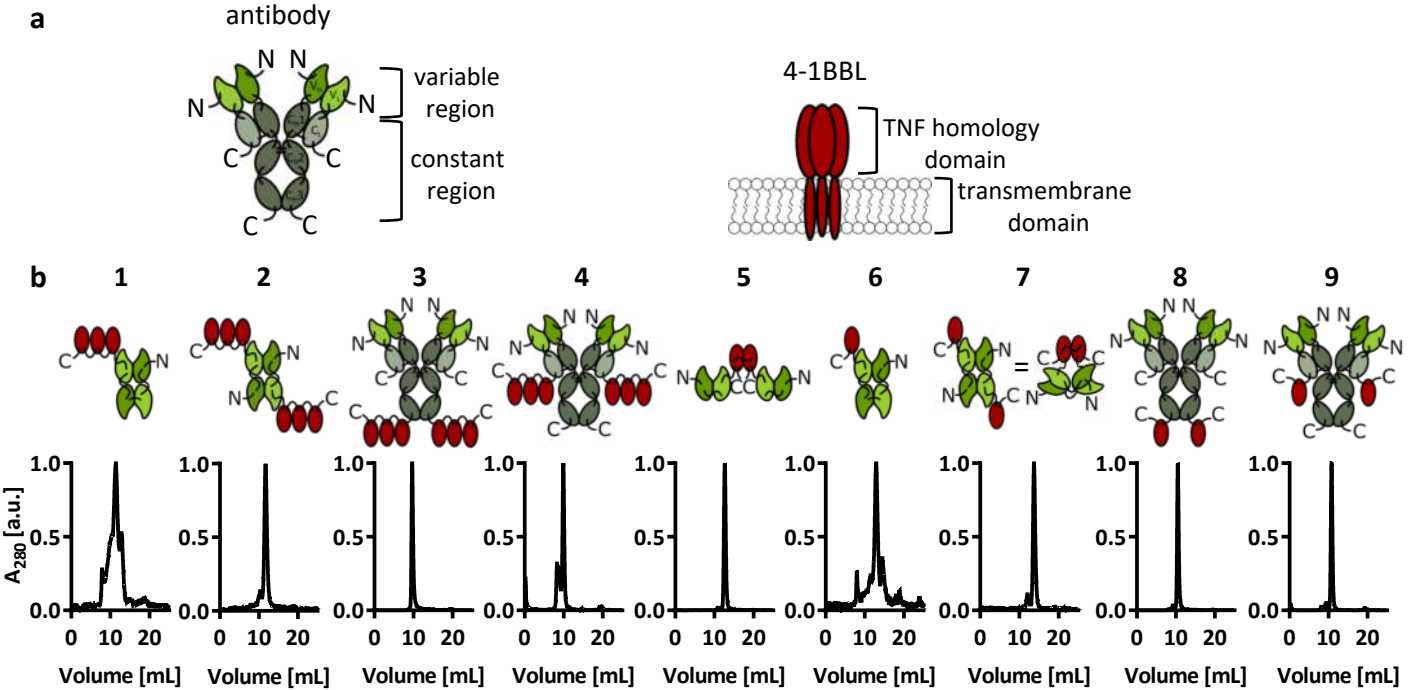
a
antibody
variable region
constant region
4-1BBL
TNF homology domain
transmembrane domain
b
1
2
3
4
5
6
7
8
9
A280 [a.u.]
1.0
0.5
0.0
0
10
20
Volume [mL]

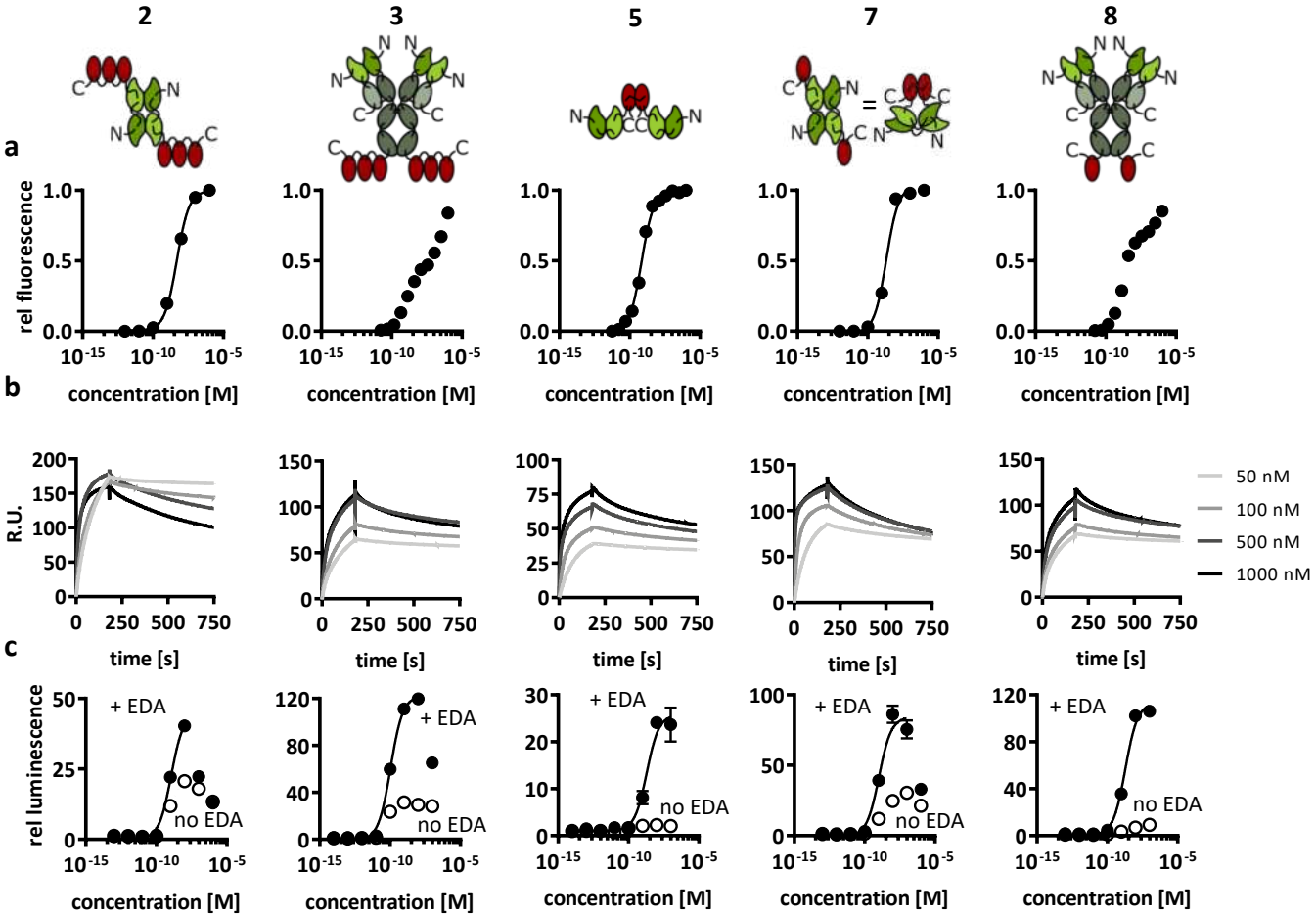
2
3
5
7
8
a
rel fluorescence
1.0
0.5
0.0
10-15
10-10
10-5
concentration [M]
b
R.U.
200
150
100
50
0
0
250
500
750
time [s]
50 nM
100 nM
500 nM
1000 nM
c
rel luminescence
50
25
120
80
40
30
20
10
100
+ EDA
no EDA

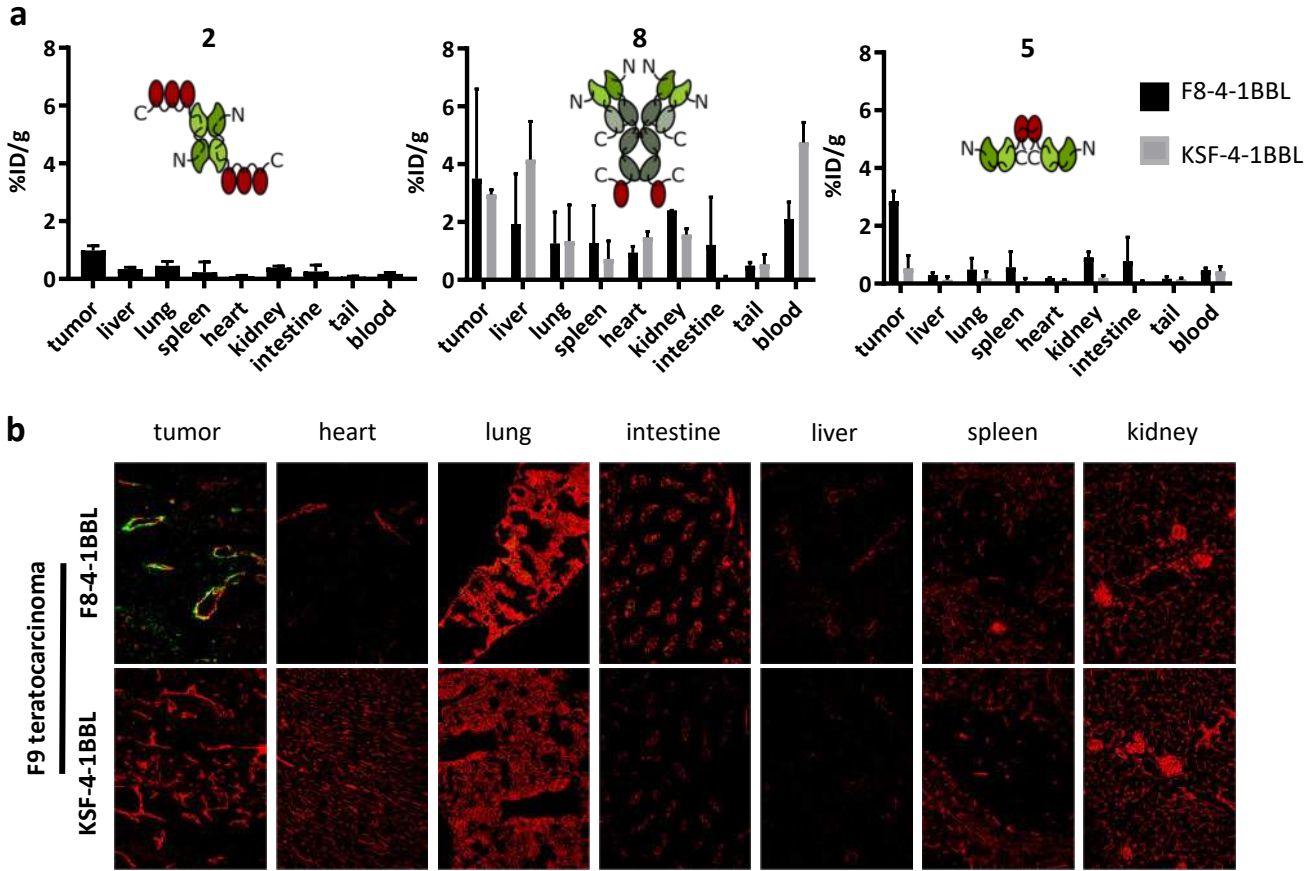
a
2
8
5
%ID/g
F8-4-1BBL
KSF-4-1BBL
tumor
liver
lung
spleen
heart
kidney
intestine
tail
blood
b
tumor
heart
lung
intestine
liver
spleen
kidney
F9 teratocarcinoma
F8-4-1BBL
KSF-4-1BBL

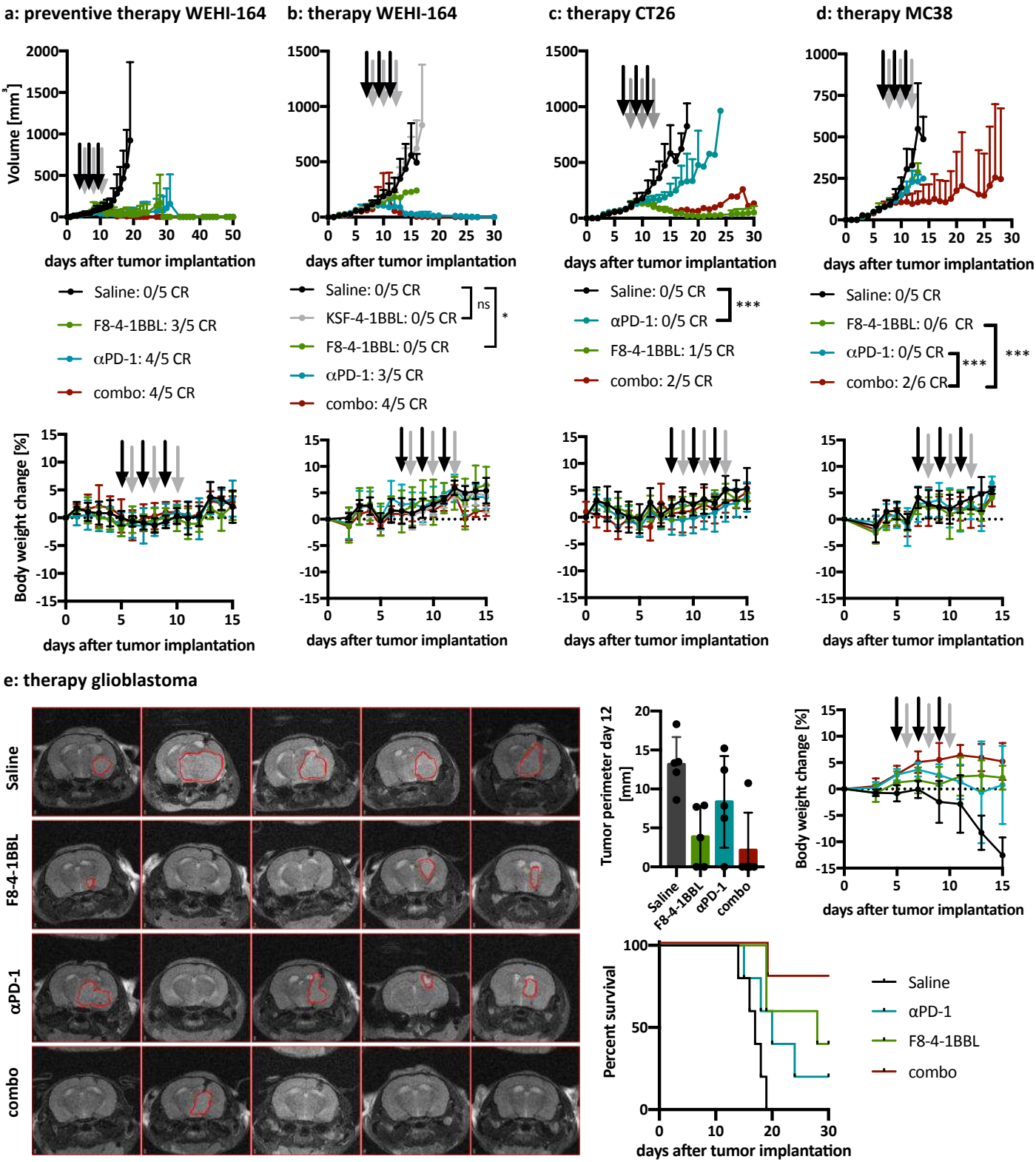
a: preventive therapy WEHI-164
b: therapy WEHI-164
c: therapy CT26
d: therapy MC38
Volume [mm³]
days after tumor implantation
Saline: 0/5 CR
F8-4-1BBL: 3/5 CR
αPD-1: 4/5 CR
combo: 4/5 CR
Saline: 0/5 CR
KSF-4-1BBL: 0/5 CR
F8-4-1BBL: 0/5 CR
αPD-1: 3/5 CR
combo: 4/5 CR
ns
*
Saline: 0/5 CR
αPD-1: 0/5 CR
F8-4-1BBL: 1/5 CR
combo: 2/5 CR
***
Saline: 0/5 CR
F8-4-1BBL: 0/6 CR
αPD-1: 0/5 CR
combo: 2/6 CR
***
***
Body weight change [%]
days after tumor implantation
e: therapy glioblastoma
Saline
F8-4-1BBL
αPD-1
combo
Tumor perimeter day 12 [mm]
Saline
F8-4-1BBL
αPD-1
combo
Body weight change [%]
days after tumor implantation
Percent survival
days after tumor implantation
Saline
αPD-1
F8-4-1BBL
combo

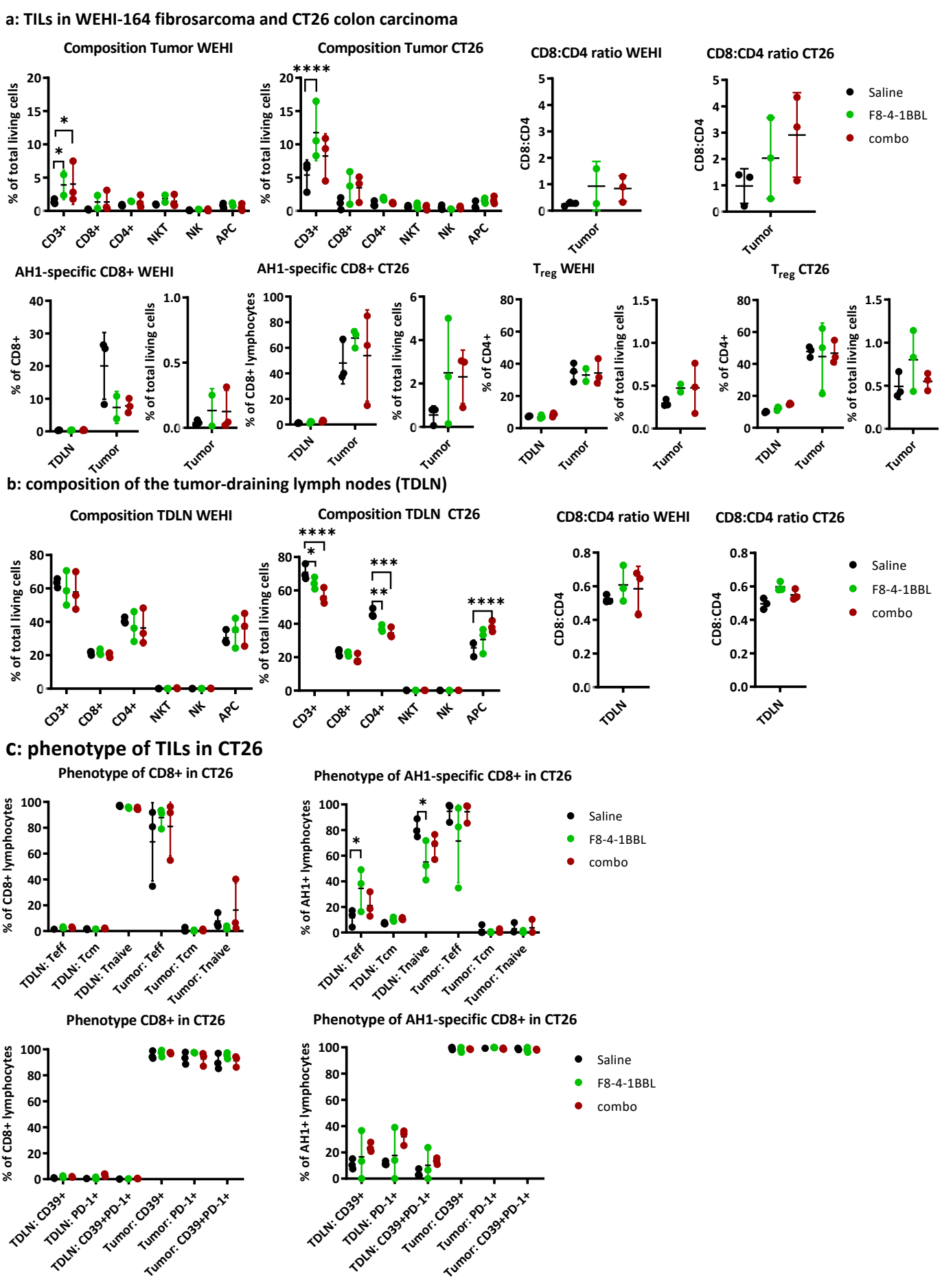
a: TILs in WEHI-164 fibrosarcoma and CT26 colon carcinoma
Composition Tumor WEHI
Composition Tumor CT26
CD8:CD4 ratio WEHI
CD8:CD4 ratio CT26
% of total living cells
CD8:CD4
CD3+
CD8+
CD4+
NKT
NK
APC
Tumor
Saline
F8-4-1BBL
combo
AH1-specific CD8+ WEHI
AH1-specific CD8+ CT26
Treg WEHI
Treg CT26
% of CD8+
% of CD8+ lymphocytes
% of CD4+
TDLN
b: composition of the tumor-draining lymph nodes (TDLN)
Composition TDLN WEHI
Composition TDLN CT26
c: phenotype of TILs in CT26
Phenotype of CD8+ in CT26
Phenotype of AH1-specific CD8+ in CT26
% of AH1+ lymphocytes
TDLN: Teff
TDLN: Tcm
TDLN: Tnaive
Tumor: Teff
Tumor: Tcm
Tumor: Tnaive
Phenotype CD8+ in CT26
Phenotype of AH1-specific CD8+ in CT26
TDLN: CD39+
TDLN: PD-1+
TDLN: CD39+PD-1+
Tumor: CD39+
Tumor: PD-1+
Tumor: CD39+PD-1+